Luminopsins integrate opto- and chemogenetics by using physical and biological light sources for opsin activation

Ken Berglund[a,b], Kara Clissold[c], Haofang E. Li[c], Lei Wen[d,e], Sung Young Park[d], Jan Gleixner[a], Marguerita E. Klein[a], Dongye Lu[c], Joseph W. Barter[c], Mark A. Rossi[c], George J. Augustine[d,e], Henry H. Yin[a,c,f,1], and Ute Hochgeschwender[a,g,h,1]

[a]Department of Neurobiology, Duke University, Durham, NC 27710; [b]Department of Neurosurgery, Emory University, Atlanta, GA 30322; [c]Department of Psychology and Neuroscience, Duke University, Durham, NC 27708; [d]Center for Functional Connectomics, Korea Institute of Science and Technology, 39-1 Hawolgokdong, Seongbukgu, Seoul 136-791, Republic of Korea; [e]Lee Kong Chian School of Medicine, Nanyang Technological University, Singapore 637553; [f]Center for Cognitive Neuroscience, Duke University, Durham, NC 27708; [g]Neuroscience Program, Central Michigan University, Mt Pleasant, MI 48859; and [h]College of Medicine, Central Michigan University, Mt Pleasant, MI 48859

Edited by Richard W. Tsien, NYU Neuroscience Institute, New York, NY, and approved December 11, 2015 (received for review June 9, 2015)

Luminopsins are fusion proteins of luciferase and opsin that allow interrogation of neuronal circuits at different temporal and spatial resolutions by choosing either extrinsic physical or intrinsic biological light for its activation. Building on previous development of fusions of wild-type *Gaussia* luciferase with channelrhodopsin, here we expanded the utility of luminopsins by fusing bright *Gaussia* luciferase variants with either channelrhodopsin to excite neurons (luminescent opsin, LMO) or a proton pump to inhibit neurons (inhibitory LMO, iLMO). These improved LMOs could reliably activate or silence neurons in vitro and in vivo. Expression of the improved LMO in hippocampal circuits not only enabled mapping of synaptic activation of CA1 neurons with fine spatiotemporal resolution but also could drive rhythmic circuit excitation over a large spatiotemporal scale. Furthermore, virus-mediated expression of either LMO or iLMO in the substantia nigra in vivo produced not only the expected bidirectional control of single unit activity but also opposing effects on circling behavior in response to systemic injection of a luciferase substrate. Thus, although preserving the ability to be activated by external light sources, LMOs expand the use of optogenetics by making the same opsins accessible to noninvasive, chemogenetic control, thereby allowing the same probe to manipulate neuronal activity over a range of spatial and temporal scales.

luciferase | bioluminescence | neural circuitry | substantia nigra | hippocampus

Optogenetics, which offers precise temporal control of neuronal activity, has been used widely in experimental neuroscience. Although optogenetic probes are indispensable tools, conventionally their application in vivo requires invasive optical fiber implants and thus imposes significant limitations for clinical applications and for applications involving multiple brain regions (1). On the other hand, chemogenetics can modulate neuronal activity throughout the brain using a genetically targeted actuator when combined with a systemically administered small molecule. Although systemic injection of a small molecule is far less invasive than implantation of fiber optics, chemogenetics has its own limitations, such as slow response kinetics and dependence on G protein signaling, which potentially elicits unwanted secondary effects in target neurons (2).

Combining the distinct advantages of opto- and chemogenetic approaches would create unprecedented opportunities for interrogation of neural circuits at a wide range of spatial scales. To allow manipulation of activity of dispersed neuronal populations using optogenetic probes without fiber-optic implants, we proposed a different approach where bioluminescence—biological light produced by enzymatic reaction between a protein, luciferase, and its diffusible substrate, luciferin—activates an opsin, which is tethered to the luciferase (3). After injection to the peripheral bloodstream, luciferin reaches a target in the brain because it crosses the blood–brain barrier (4). Light is generated by the luciferase and then activates the opsin, resulting in activation (in case of channelrhodopsins) or inhibition (in case of proton or chloride pumps) of the target neurons. Capitalizing on the major advantage of opsins as powerful generators of electrical current, our approach integrates opto- and chemogenetic methods by preserving conventional photoactivation of opsins where desired, while at the same time providing chemogenetic access to the same molecules, thus allowing manipulation of neuronal activity over a range of spatial and temporal scales in the same experimental animal.

Initial proof-of-concept studies showed that *Gaussia* luciferase (GLuc)-emitted light is able to activate opsins when the two molecules are fused together (luminescent opsin or luminopsin, LMO) (3). Here we report a set of new LMOs, incorporating brighter versions of GLuc, with significantly improved performance. We found that the improved LMOs could modulate neuronal activity via bioluminescence in vitro, ex vivo, and in vivo and could elicit behaviors in freely moving mice.

Results

Determining Light Intensity Required for Inducing Action Potentials. We previously reported that LMO2, a luminopsin based *on Volvox* channelrhodopsin 1 (VChR1) (5, 6), generates subthreshold

Significance

Although conventional optogenetics utilizing microbial photosensitive channels or pumps to control activity of neurons has enabled great progress in neuroscience, reliance on delivery of light by optic fibers implanted into the brain imposes certain logistical burdens and thus limits application of optogenetics. To expand their utility, we fused optogenetic probes with luciferase that emits biological light in the presence of a substrate and showed that the activity of neurons in vitro, ex vivo, and in vivo could be controlled by biological light in addition to physical light. Such fusion proteins, termed luminopsins, could prove invaluable for experimental and clinical neuroscience.

Author contributions: K.B., G.J.A., H.H.Y., and U.H. designed research; K.B., K.C., H.E.L., L.W., S.Y.P., J.G., and U.H. performed research; M.E.K. contributed new reagents/analytic tools; K.B., K.C., H.E.L., L.W., S.Y.P., J.G., D.L., J.W.B., M.A.R., G.J.A., H.H.Y., and U.H. analyzed data; and K.B., G.J.A., H.H.Y., and U.H. wrote the paper.

The authors declare no conflict of interest.

This article is a PNAS Direct Submission.

Freely available online through the PNAS open access option.

[1]To whom correspondence may be addressed. Email: ute.hochgeschwender@cmich.edu or hy43@duke.edu.

This article contains supporting information online at www.pnas.org/lookup/suppl/doi:10.1073/pnas.1510899113/-/DCSupplemental.

depolarizations upon application of coelenterazine (CTZ), a substrate for GLuc (3). To determine the light intensity required for the VChR1 moiety within LMO to induce action potential firing, we illuminated a neuron with blue light (465–495 nm, which covered most of the emission spectrum of GLuc) (Fig. 1*A*). The amount of depolarization produced by 1-s light flashes increased with increasing light intensity, reaching action potential threshold at light intensities above 10 μW/mm^2. The relationship between light intensity and action potential frequency could be fitted by the Hill equation (Fig. 1*B*; $n = 8$), and the minimal light intensity that induced at least one spike was 33 ± 13 μW/mm^2 (mean ± SEM; $n = 8$). Thus, to reliably produce action potentials, it is necessary to have a luciferase that can emit sufficient bioluminescence.

Identifying a GLuc Variant That Emits More Light. To identify a variant of luciferase that emits more photons, we compared wild-type GLuc (7, 8) to its variants "superluminescent" (slGLuc) (9), and "slow-burn" (sbGLuc) (10), as well as to NanoLuc (11, 12), a luciferase engineered from *Oplophorus gracilirostris*. Each luciferase was fused to the extracellular N terminus of VChR1 and thus expressed on the extracellular surface of transfected HEK cells; the fluorescent reporter EYFP was fused to the C terminus of VChR1, allowing identification of transfected cells. When treated with different doses of the GLuc substrate CTZ, bioluminescence reached a peak within a minute after addition of CTZ and decayed afterward, halving in the first 5–10 min and becoming negligible after 1 h. At all CTZ concentrations tested, sbGLuc showed the largest bioluminescence (Fig. 1 *C* and *D*). To quantify the dose–response relationships shown in Fig. 1*C*, luminescence from each luciferase was fitted with the Hill equation (Fig. 1*C*). Although EC_{50} values for the different luciferases were similar (92, 74, 51, and 12 μM for GLuc, slGLuc, sbGLuc, and NanoLuc, respectively), the maximal luminescence emitted by each was quite different [49, 110, 220, and 9 (× 10^6 photons/s/cm^2/sr) for GLuc, slGLuc, sbGLuc, and NanoLuc, respectively]. To facilitate comparison of the different constructs, Fig. 1*D* shows bioluminescence evoked by a 50-μM concentration of CTZ, which is the estimated plasma level in a mouse receiving an i.v. injection of 50 μg CTZ. At this concentration, sbGLuc emitted about 10 times more photons than wild-type GLuc. NanoLuc did not respond to CTZ very well but did respond to its own substrate, furimazine; the resulting luminescence was smaller than that of sbGLuc (activated by CTZ) but comparable to that of slGLuc. Thus, NanoLuc does not have significant chemical cross-talk with GLuc, making it suitable for simultaneous use of two different luminopsins. Based on these results, we decided to further characterize LMOs with the sbGLuc and slGLuc variants.

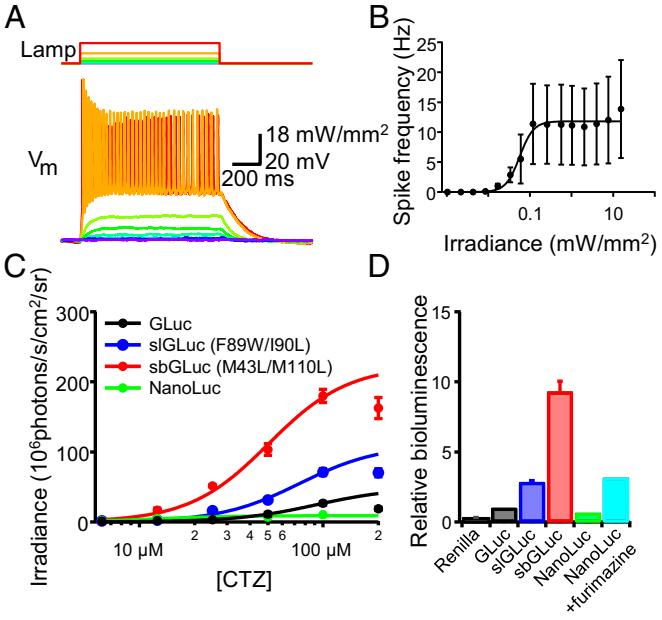

Fig. 1. Determining minimum light intensity for induction of action potential for *Volvox* channelrhodopsin 1 and comparison of light emission from variants of GLuc. (*A*) A cortical neuron from a rat embryo in culture expressing *Volvox* channelrhodopsin 1 (VChR1) was whole-cell current-clamped and light pulses (1 s, 480 nm) at different intensities were delivered, resulting in sub- and suprathreshold depolarizations. (*B*) Frequency of action potential firing was quantified as a function of light intensity. Fitting with the Hill equation resulted in maximum firing frequency of 11.8 ± 0.3 Hz, half-maximum light intensity of 56.7 ± 5.1 μW/mm^2, and the Hill coefficient of 2.6 ± 0.6. $n = 8$. Error bars indicate SEM in this and subsequent figures. (*C*) HEK cells were transfected with wild-type GLuc, super luminescent (slGLuc), and slow burn (sbGLuc) variants, and with NanoLuc luciferase all fused with VChR1, and were challenged with different concentrations of CTZ to obtain dose–response curves for bioluminescence using a plate reader. The data were fitted with the Hill equations. Hill coefficients were set to 2. $n = 3$ wells. (*D*) sbGLuc showed a ∼10-fold increase in bioluminescence compared with wild-type GLuc at a 50 μM CTZ concentration. Luminescence from *Renilla* luciferase and from NanoLuc with its own substrate, furimazine, was also plotted. The same dataset obtained from HEK cells shown in *C* was replotted. $n = 3$ wells.

Increased Bioluminescence Improves Coupling Efficiency Between Luciferase and Opsin. The performance of wild-type and slow burn GLuc was compared in HEK cells by measuring the CTZ-induced current under whole-cell patch clamp (Fig. 2*A*). With LMO1 and LMO2, which are combinations of wild-type GLuc and ChR2 (LMO1) and VChR1 (LMO2), we observed small inward currents upon application of CTZ. When GLuc was replaced in LMO2 with the brighter variant sbGLuc, to produce LMO3, the inward current induced by CTZ treatment was markedly larger (Fig. 2*A*).

To further quantify the performance of the three LMOs, we examined the amount of current induced by CTZ application and compared it to the current induced by maximal activation by light from the lamp (Fig. 2*B*). For each variant of luminopsin, there was a positive correlation between the two: Higher surface expression of the channel, reflected in larger amplitudes of lamp-induced currents, was associated with a larger CTZ-induced current. The slopes of these relationships indicate that LMO3 was able to activate channels most effectively upon CTZ application. Surface expression levels, assessed via the amplitude of lamp-induced photocurrents, was similar ($P = 0.19$; two-tailed Student's *t* test): 1,042 ± 168 pA for LMO2 (mean ± SEM, $n = 10$) and 993 ± 185 pA ($n = 14$) for LMO3. We observed similar correlations between the photocurrent and CTZ-induced current in LMO3-expressing neurons in brain slice preparations (Fig. 2*B*, open red symbols). To quantify this difference, we measured the coupling efficiency, which is the amplitude of current induced by a saturating dosage of CTZ (100 μM; see Fig. 1*C*) divided by that of the photocurrent induced by a saturating intensity of lamp (1 mW/mm^2; see Fig. 1*B*); this represents the fraction of channels that can be activated by CTZ (Fig. 2*C;* see ref. 3). LMO3 had a coupling efficiency ∼10-fold higher than that of LMO2, with over 10% of the VChR1 channels activated by CTZ treatment.

Increased Bioluminescence Controls Action Potential Firing. The improved performance of LMO3 suggests that it could be better than LMO1 or LMO2, which are not effective in evoking action potential firing in response to CTZ application (3). To test the ability of LMO3 to manipulate neuronal activity, we expressed it in dissociated cortical neurons in culture. Cultured neurons were transfected with LMO3 under the control of the CAG promoter. Upon application of CTZ, LMO3-expressing neurons showed

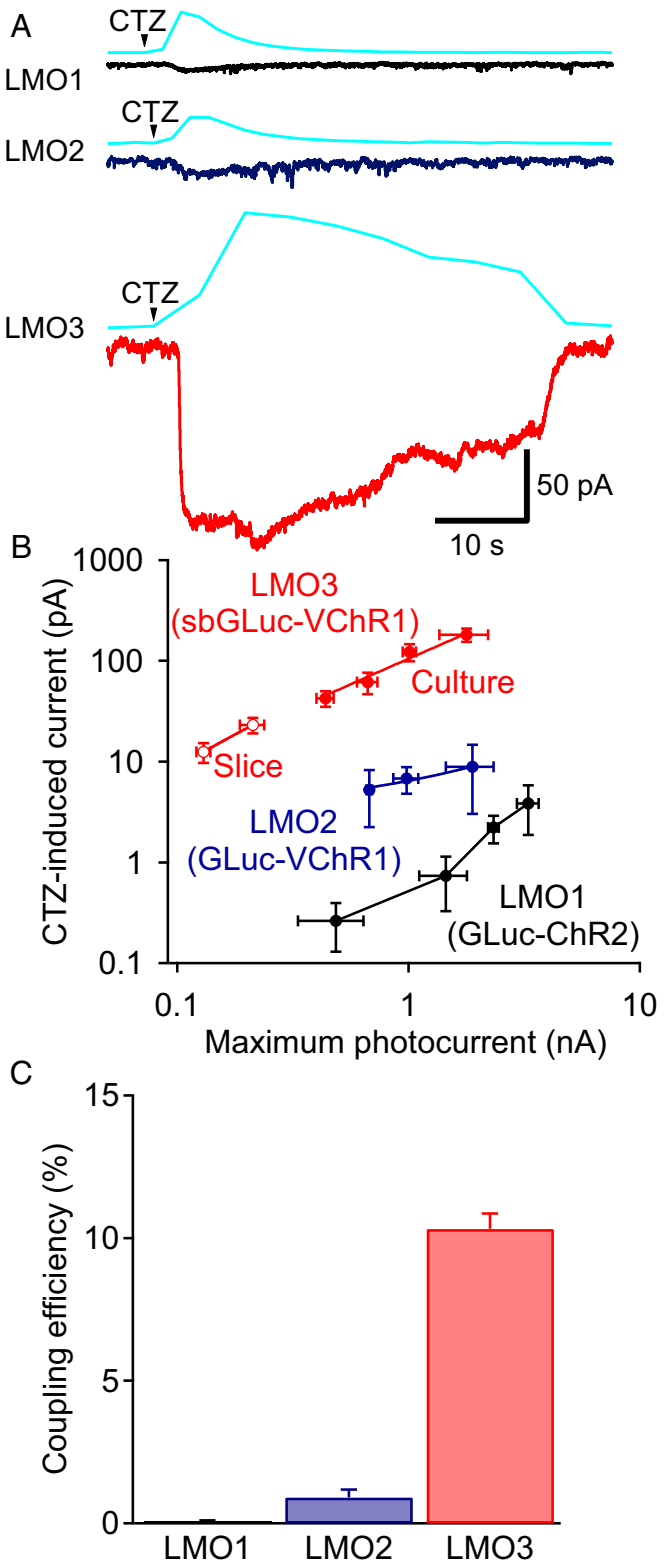

Fig. 2. Luciferases with higher light emission improve coupling efficiency. (*A*) Representative CTZ-induced currents with LMO1 (GLuc-ChR2; *Top*), LMO2 (GLuc-VChR1; *Middle*), and LMO3 (sbGLuc-VChR1; *Bottom*) in transfected HEK cells (sampling rate, 10 KHz). Bioluminescence was obtained simultaneously but at a much lower sampling rate (0.2 Hz) and is shown in the same scale for the three examples (cyan). (*B*) For all LMOs, the response to CTZ correlated with the maximum photocurrent elicited by direct illumination. However, for a given value of maximum photocurrent, responses to CTZ were higher for cells expressing LMO2 than for cells expressing LMO1 and substantially higher for cells expressing LMO3. n = 3–4 cells for each data point from 12 (LMO1; HEK cells), 10 (LMO2; HEK cells), and 14 (LMO3; neurons in culture) cells in total. The correlation between photocurrent and CTZ-induced current was also examined in the brain slice preparation (open symbols in red; n = 3 and 4 cells). (*C*) The efficiency of coupling between the GLuc variants and the channelrhodopsins was calculated from the same dataset shown in *B* by dividing the amplitude of the CTZ-induced current by that of the maximum photocurrent induced by direct illumination of the LMOs. The coupling efficiency of LMO3 was significantly higher than that of the first two LMOs. n = 12 (LMO1), 10 (LMO2), and 21 (LMO3). The coupling efficiency of LMO3 determined in neurons in culture and in brain slice preparation was not significantly different (P = 0.87; two-tailed unpaired Student's t test; n = 14 and 7 for culture and slice preparation, respectively) and thus pooled together.

robust bioluminescence in their cell bodies as well as throughout their processes (Fig. 3*A*). The bioluminescence induced by CTZ activation of LMO3 was sufficient to produce suprathreshold depolarization of the neuronal membrane potential and could induce action potential firing (Fig. 3*B*). The mean CTZ-induced depolarization of LMO3-expressing neurons was more than 10 mV, whereas it was less than 5 mV in LMO2-expressing neurons (Fig. 3*E*). Thus, sbGLuc was able to emit bioluminescence that activated the VChR1 moiety sufficiently to induce neuronal action potential firing. This is a significant qualitative improvement in performance over earlier LMOs (3).

We further extended the luminopsin concept to inhibition of neuronal activity by incorporating an inhibitory opsin. For this purpose, we first tested the suitability of a photosensitive proton pump from the fungus *Leptosphaeria maculans* (Mac) (13) for activation by GLuc emission. We transfected neurons with a fusion protein of Mac-EGFP and slGLuc, which we termed iLMO, and compared the photosensitivity of iLMO to blue light (480 nm) and other wavelengths (Fig. S1). Although iLMO was more sensitive to longer wavelengths, it also showed substantial sensitivity to 480-nm light, suggesting possible activation by GLuc emission. Thus, we further tested iLMO in cortical neurons in culture (Fig. 3 *C*–*E*). Similar to LMO3, iLMO-expressing neurons showed robust bioluminescence in their cell bodies and processes (Fig. 3*C*). To examine the ability of iLMO to inhibit action potential firing, action potentials were elicited by repetitive injection of threshold-level currents at 1 Hz (Fig. 3*D*). CTZ application caused bioluminescence and concomitant hyperpolarization and abolished action potential firing. Similar results were obtained in four cells in total where CTZ caused small but significant hyperpolarization (Fig. 3*E*), on average, equivalent to 63% (–4.3 ± 1.0 mV; mean ± SEM; n = 4 cells) of the hyperpolarization induced by lamp illumination (4 mW/mm^2). Thus, in addition to excitatory LMOs, inhibitory LMOs can harness bioluminescence at relatively high efficiency to inhibit neuronal action potential firing. Another form of inhibitory luminopsin based on engineered *Renilla* luciferase and an inhibitory, light-driven chloride pump, *Natronomonas* halorhodopsin, has just been reported (14).

Bioluminescence Activates Synaptic Networks in Vitro. The small diameter of an optical fiber limits delivery of light, so that conventional optogenetic probes can affect only a relatively small number of neurons. One of the potential advantages of LMOs is that their diffusible small-molecule substrate (e.g., CTZ) allows control of a large or dispersed population of neurons that would otherwise be beyond the reach of optical fibers. To illustrate this, we infected entire populations of neurons on a coverslip with either lenti or adeno-associated virus (AAV) carrying the LMO3 gene under control of the human synapsin promoter (hSyn), choosing a virus titer that yielded transduction of most neurons by LMO3. The effects of CTZ were compared with that of an arc lamp under these conditions (Fig. 4). Whole-cell patch clamp recordings were made from LMO3-negative cells (red cell in Fig. 4*A*), based on the absence of LMO3 fluorescence in the

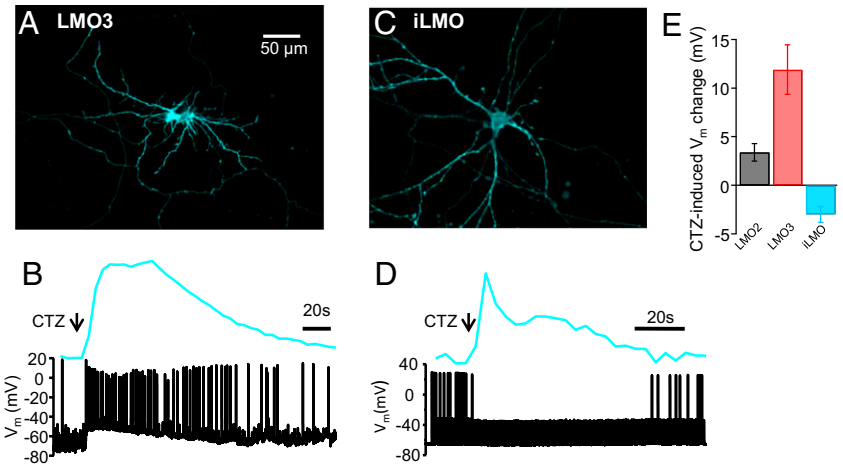

Fig. 3. Bioluminescence controls action potential firing. (*A*) An LMO3-expressing neuron showed bioluminescence upon CTZ application (100 μM). (*B*) CTZ-induced bioluminescence (blue trace) in the LMO3-expressing neuron shown in *A* caused depolarization and action potential firing (black trace). (*C*) An iLMO-expressing neuron showed bioluminescence upon CTZ application (100 μM). (*D*) CTZ-induced bioluminescence (blue trace) in an iLMO-expressing neuron caused slight hyperpolarization and inhibition of action potential firing (black trace). Action potentials were induced by peri-threshold depolarizing currents (60 pA, 15 ms) at 1 Hz. (*E*) Mean membrane potential change caused by CTZ application in neurons expressing LMO2, LMO3, and iLMO. n = 8, 4, and 4, respectively.

plasma membrane. Cells were held near the reversal potential for Cl^- to isolate excitatory postsynaptic currents (EPSCs). Surrounding neurons were stimulated with a spot of light (670 μm diameter) from an arc lamp (Fig. 4*A*) covering less than 0.6% of the total area of the coverslip (9 mm in diameter). Fast and transient EPSCs, together with negligible slow and sustained direct photocurrents in some cells, were recorded during photostimulation with the light spot (Fig. 4*B*). These currents were glutamatergic because they were blocked by application of the glutamate receptor antagonists, CNQX (100 μM) plus kinurenic acid (3 mM; Fig. 4*C*). Next, to activate the entire population of neurons on the coverslip, CTZ (100 μM, 470 μL) was added to the recording chamber. This generated bioluminescence that lasted for tens of seconds in all observable LMO3-transduced cells (Fig. 4*D*) and elicited widespread network activity, recorded as a barrage of EPSCs (Fig. 4*E*). On average, the frequency of spontaneous EPSCs was significantly increased both by the light spot and by CTZ (Fig. 4*F*; $^*P < 0.05$; paired Student's t test; $n = 8$). Averaged EPSC waveforms were similar between spot- and CTZ-induced EPSCs (Fig. 4*G*), indicating that the two methods activated the same presynaptic inputs. These results indicate that the optogenetic element in LMO3 can be activated by both physical and biological light sources and that CTZ can provide sufficient excitatory drive to induce action potentials in a population of neurons within a network.

Bioluminescence Controls Neuronal Activity and Behavior in Vivo. To test the applicability of bioluminescence-driven optogenetics in mice in vivo, we used an established behavioral paradigm. Unilateral activation of GABAergic neurons in the substantia nigra pars reticulata (SNr) induces ipsiversive circling behavior, whereas silencing the same neurons induces contraversive circling (15). Based on previous studies using pharmacological and lesion perturbations (15), it is shown that this circling behavior reflects the relative strength of outputs from the two sides of the SNr. We therefore used circling as a behavioral readout for unilateral nigral manipulation via LMOs.

We first injected AAV expressing LMO3 (AAV-hSyn-LMO3) into the SNr and characterized virus-transduced neurons via whole-cell patch clamp recordings in acute SNr slices (Figs. S2 and S3). We recorded from four LMO3-positive SNr neurons; these were identified as principal GABAergic cells (the vast majority of neurons in the SNr) (16–18) due to minimal voltage "sag" in response to hyperpolarizing currents (Fig. S2*A*). In these cells, LMO3 expression was sufficiently robust to induce action potential firing in response to light (Fig. S2*B*). This allowed us to use a scanned laser spot to map the light sensitivity of these cells (Fig. S2 *C* and *D*). Moreover, in one cell, we observed an increase in the frequency of fast outward currents, presumably representing GABAergic inhibitory postsynaptic currents (IPSCs), in response to both lamp photostimulation and CTZ application (Fig. S3). Given that principal cells express LMO3 and are known to send GABAergic collaterals to neighboring cells (17–19), these IPSCs presumably resulted from activation of these local connections. Taken together, these results indicate that AAV-hSyn-LMO3 is expressed in GABAergic cells in the SNr and that activation of LMO3 can cause action potential firing in these cells.

We next asked whether LMOs could alter neuronal activity in the SNr of intact animals. We injected AAV-hSyn-LMO, either activating (LMO3; $n = 5$ mice) or inhibiting (iLMO; $n = 5$ mice), into the SNr of mice. Six to 10 wk after injection, we implanted multielectrode arrays to record the activity of SNr neurons in awake mice chronically. Approximately 2 wk after electrode implant surgery, mice received i.p. injections of either CTZ (200 μg in 200 μL PBS per 30 g animal) or PBS, whereas firing of SNr neurons was recorded for 1 h starting 30 min before injection until 30 min after injection. Recordings were carried out daily, alternating the order of injections (CTZ vs. vehicle) between animals.

Representative recordings of the activity of well-isolated units from mice expressing AAV-hSyn-LMO3 (Fig. 5*A*) and AAV-hSyn-iLMO (Fig. 5*C*) showed relatively high levels of spontaneous activity characteristic of SNr GABAergic neurons. Firing rates before and after CTZ injection are shown in Fig. 5 B and *D*. In mice expressing AAV-hSyn-LMO3, a two-way ANOVA with time and group as factors showed an interaction between these factors, $F(1, 59) = 4.29$, $^*P = 0.044$. Post hoc tests (Bonferroni) showed an increased firing rate postinjection of CTZ compared with preinjection ($^*P = 0.0020$), but no effect for vehicle injection was observed ($P = 0.76$). In mice expressing AAV-hSyn-iLMO, the average firing rates after CTZ injection decreased following CTZ injection [interaction for two-way ANOVA, $F(1, 80) = 6.78$, $^*P = 0.01$; post hoc comparison between pre and post, $^*p = 0.0003$ for CTZ injection, $n = 46$, $P = 0.91$ for vehicle injection, $n = 36$].

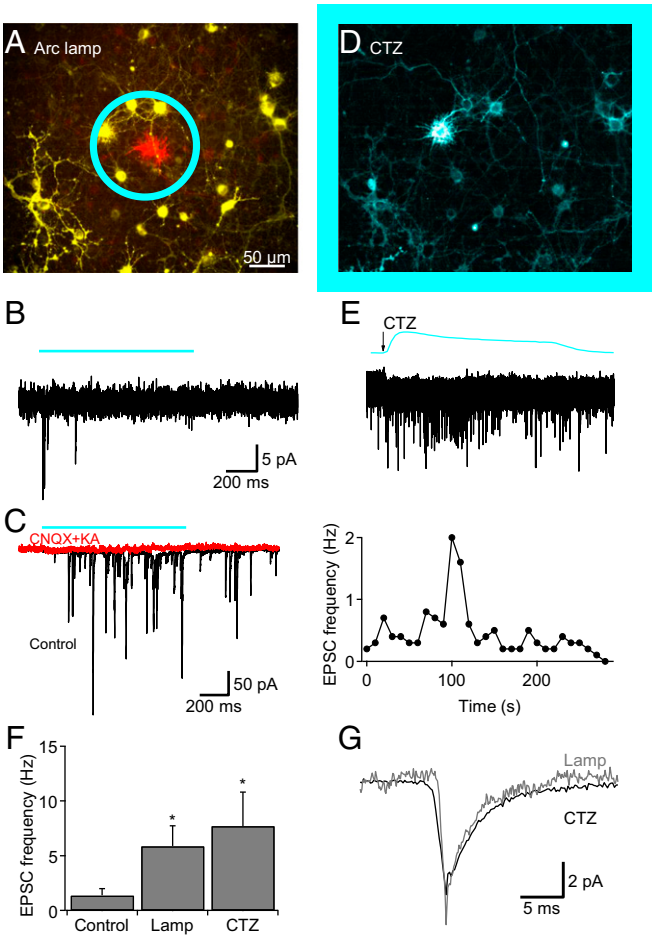

Fig. 4. Bioluminescence elicits postsynaptic currents in vitro. (*A*) Cortical neurons from rat embryos in culture were transduced by lentivirus carrying the LMO3 gene, resulting in EYFP tag expression (yellow). A negative cell in the center was whole-cell patch clamped and filled with Texas Red dye (shown in red), whereas neighboring cells were activated by focal photostimulation with an arc lamp depicted as a cyan circle (not scaled; the actual spot size in wide-field illumination was 670 μm in diameter). (*B*) A light pulse (1 s; 480 nm; 1 mW/mm^2; 670 μm in diameter) elicited fast inward currents in the cell under voltage clamp at −60 mV. The internal solution contained 12.5 mM chloride to keep the equilibrium potential of chloride close to the holding potential. (*C*) In another cell, fast inward currents elicited by photostimulation were blocked by a mixture of ionotropic glutamate antagonist, CNQX (100 μM) and kinurenic acid (KA; 3 mM), indicative of glutamatergic EPSCs. (*D*) CTZ (100 μM; 470 μL) was bath-applied to the same coverslip shown in *A*, causing widespread bioluminescence. Bioluminescence was expected in the entire coverslip (9 mm in diameter) depicted as a cyan rectangle (not scaled). (*E*) CTZ-induced bioluminescence (blue trace, *Top*) caused fast inward currents (black trace, *Middle*) while it lasted. EPSC frequency was quantified in 10-s bins (*Bottom*). All traces are shown in the same time scale. (*F*) Mean frequency of spontaneous EPSCs before stimulation (control), during stimulation by lamp, or by CTZ (*$P < 0.05$; paired Student's *t* test; $n = 8$ for both lamp and CTZ). (*G*) Averaged waveforms of EPSCs recorded from the cell shown in *A*, *B*, and *E* during photostimulation by lamp and by bioluminescence with CTZ. $n = 24$ (lamp) and 101 (CTZ).

To examine how long CTZ injection remains effective, two mice (one with LMO3 and the other with iLMO) received both PBS and CTZ in the same session, and firing of SNr neurons was recorded for 2 h after each injection. This allowed us to estimate the offset times for the effect of CTZ in the same neurons. As shown in Fig. 5*E*, the effects of CTZ on neuronal firing rate started immediately and lasted up to 45 min. To analyze these data statistically, we divided the postinjection period into two epochs (0-45 min and 46–120 min) and compared the firing rates using a two-way ANOVA, with group (CTZ and vehicle) and time (epoch 1 and epoch 2). There was a significant interaction between group and time for LMO3, $F(1, 14) = 14.97$, *$P = 0.0017$, $n = 8$. Post hoc tests showed CTZ injection only increased firing rates relative to controls in the first epoch (*$P = 0.0020$) but not in in the second—that is, after 45 min ($P = 0.53$). For iLMO, there was also a significant interaction between group and time, $F(1, 22) = 12.93$, *$P = 0.0016$, $n = 12$. Again, post hoc tests showed CTZ injection is only effective in the first epoch (*$P = 0.0018$) but not in in the second—that is, after 45 min ($P = 0.64$). These results indicate that, in mice expressing LMO3 or iLMO, i.p. injections of CTZ can bidirectionally control the activity of target neurons in the SNr for ∼45 min.

Finally, we examined the behavioral effects of LMO activation (Fig. 6). AAVs expressing either the excitatory LMO3 (Fig. 6 *A*, left two panels, and B) or inhibitory iLMO (Fig. 6 *A*, right two

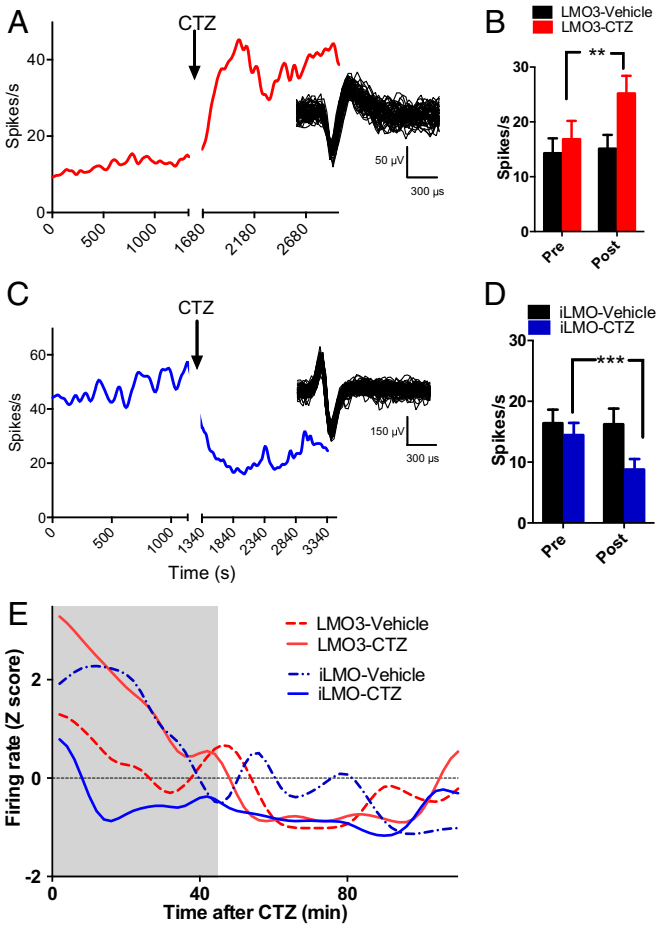

Fig. 5. Bioluminescence changes in vivo single unit activity bidirectionally in awake behaving mice. (*A*) Firing rate of a representative neuron in the SNr that increased firing after CTZ in a mouse expressing LMO3, with its spike waveform on the right. (*B*) LMO3 population summary: average firing rates before and after injection [**$P < 0.01$; two-way ANOVA followed by post hoc test; $n = 30$ (vehicle) and 31 (CTZ) cells from 5 mice]. Error bars represent SEM. (*C*) Firing rate of a representative SNr neuron that decreased firing after CTZ in a mouse expressing iLMO, with its spike waveform on the right. (*D*) iLMO population summary: average firing rates before and after injection [***$P < 0.001$; two-way ANOVA followed by post hoc test; $n = 36$ (vehicle) and 46 (CTZ) cells from five mice]. (*E*) Firing rates of two representative neurons over 2 h following injection of CTZ (1 for LMO3 and 1 for iLMO). Shaded area indicates the estimated period during which CTZ remains effective in altering firing rates.

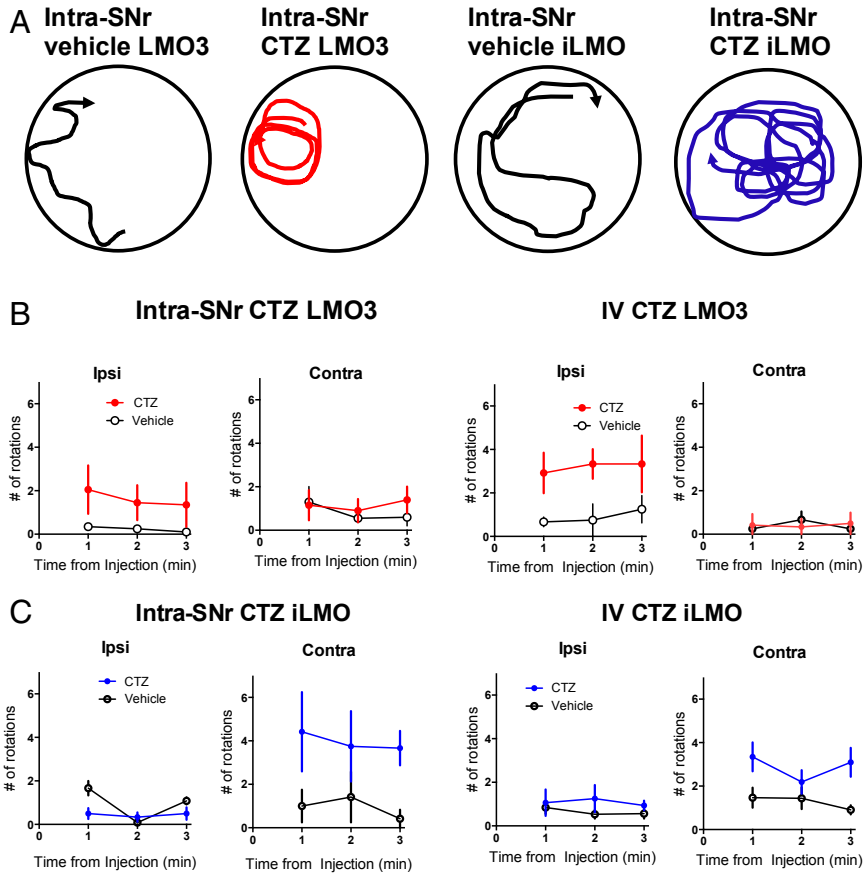

Fig. 6. Bioluminescence modulates behavior in awake freely moving mice. (*A*) Representative trajectories of mouse bodies showing effects of intra-SNr injection of CTZ on turning behavior in mice expressing LMO unilaterally in the SNr. Unilateral excitation of nigral neurons produced more ipsiversive turning (LMO3), whereas unilateral inhibition produced more contraversive turning (iLMO), consistent with well-established observations of nigral functions. (*B*) In mice expressing LMO3, injection of CTZ into the SNr ($n = 3$) or the tail vein ($n = 5$) increased ipsiversive turning ($^*P = 0.0021$ and $^*P = 0.04$, respectively; two-way ANOVA followed by post hoc test). (*C*) In mice expressing iLMO, injection of CTZ into the SNr ($n = 3$) or the tail vein ($n = 8$) increased contraversive turning ($^*P = 0.016$ and $^*P = 0.0003$, respectively; two-way ANOVA followed by post hoc test).

panels, and C) were delivered to the left SNr of mice through implanted cannulas. After 3–5 wk, we quantified and compared circling behavior under two conditions: direct application of CTZ through the cannula (Fig. 6 *B* and *C*, left two panels), and systemic application of CTZ by i.v. injection (Fig. 6 *B* and *C*, right two panels). For both routes of application, PBS was used as a vehicle control.

When CTZ was directly injected into the SNr through a cannula (34 ng in 0.4 μL; $n = 3$), mice expressing AAV-hSyn-LMO3 showed more ipsiversive turns, as expected when GABAergic SNr neurons are excited. A two-way ANOVA on ipsiversive turns from the first 3 min showed no interaction between CTZ and time, $F(2, 6) = 0.11$, $P = 0.90$; no main effect of time, $F(2, 6) = 0.12$, $P = 0.89$; but a significant main effect of CTZ, $F(1, 6) = 26.81$, $^*P = 0.0021$. By contrast, there was no main effect of CTZ on contraversive turns, $F(1, 6) = 0.034$, $P = 0.86$, or any interaction between CTZ and time, $F(2, 6) = 1.48$, $P = 0.30$. Similar effects were observed when CTZ was applied through the tail vein (200 μg in 50 μL; $n = 5$). For ipsiversive turns, there was no interaction between CTZ and time, $F(2, 12) = 0.07$, $P = 0.93$; no main effect of time, $F(2, 12) = 0.27$, $P = 0.77$; but a significant main effect of CTZ, $F(1, 12) = 5.28$, $^*P = 0.04$. For contraversive turns, there was no interaction, $F(2, 16) = 0.68$, $P = 0.52$; no main effect of time, $F(2, 16) = 0.75$, $P = 0.49$; or no main effect of CTZ, $F(1, 8) = 0.28$, $P = 0.61$.

Mice expressing AAV-hSyn-iLMO injected with CTZ into the SNr through a cannula showed more contraversive turns, as expected when SNr neurons are inhibited ($n = 3$). A two-way ANOVA on ipsiversive turns from the first 3 min showed an interaction between CTZ and time, $F(2, 6) = 7.55$, $P = 0.02$; a marginal main effect of time, $F(2, 6) = 4.9$, $P = 0.053$; and a significant main effect of CTZ, $F(1, 6) = 11.17$, $^*P = 0.016$. A post hoc analysis showed that the vehicle controls had more ipsiversive turns during the first minute ($^*P < 0.05$). By contrast, for contraversive turns, there was no interaction between CTZ and time, $F(2, 6) = 0.37$, $P = 0.71$; no main effect of time, $F(2, 6) = 0.10$, $P = 0.9$; but a significant main effect of CTZ, $F(1, 6) = 29.3$, $^*P = 0.0016$. Similar effects were observed when CTZ was applied through the tail vein (200 μg in 50 μL; $n = 8$). For ipsiversive turns, there was no interaction between CTZ and time, $F(2, 21) = 0.15$, $P = 0.85$; no main effect of time, $F(2, 21) = 0.18$, $P = 0.83$; and no main effect of CTZ, $F(1, 21) = 1.35$, $P = 0.26$. For contraversive turns, there was no interaction between CTZ and time, $F(2, 21) = 1.35$, $P = 0.28$; no main effect of time, $F(2, 21) = 0.52$, $P = 0.60$; but there was a significant main effect of CTZ, $F(1, 21) = 18.24$, $^*P = 0.0003$.

Thus, i.v. injections of CTZ produced similar effects as local injection into the SNr. Regardless of how CTZ was applied, the activation of LMO3 and iLMO produced consistent effects on turning behavior in mice: ipsiversive turning due to excitation of SNr neurons and contraversive turning due to inhibition of SNr neurons, respectively. Interestingly, the behavioral effects of CTZ (up to 4 min) did not last nearly as long as the effects on neural activity (up to 45 min). One possible explanation for this

difference is that there were compensatory changes in other areas (e.g., contralateral SNr) in response to long-lasting effects on neural activity, to resist continuous turning behavior.

In summary, these results demonstrate that the luciferase substrate CTZ reaches the brain when injected in the periphery and generates bioluminescence sufficient to activate opsins and initiate specific motor behavior in mice without requiring optical fibers to activate the opsins.

Bimodal Opto- and Chemogenetic Interrogation of the Same Circuit by Luminopsin. The same synaptic circuit analyzed by LMO3 in behaving animals in vivo also can subsequently be interrogated, using tissue from the same animal, for higher resolution analysis ex vivo. To demonstrate this bimodal utility of LMOs, AAV-hSyn-LMO3 was injected into the hippocampus of mice and 4 wk later slices were prepared (Fig. 7).

Current-clamp recordings were used to define the ability of CTZ to excite LMO3-expressing neurons in CA3. The resting membrane potential of these cells was –64.1 ± 1.0 mV (mean ± SEM; $n = 6$ cells). Although CTZ application depolarized all six CA3 neurons examined, the amplitude of CTZ-induced depolarization was somewhat smaller than observed in cultured hippocampal neurons, reflecting smaller photocurrents (and lower LMO3 expression) in the brain slice preparation (Fig. 2*B*). As a result, the mean CTZ-induced depolarization of 8.9 mV ± 4.6 mV (mean ± SEM; $n = 6$ cells) was below the threshold for action potential firing (–38.8 mV ± 0.8 mV; mean ± SEM; $n = 6$ cells) in most cases; thus, CTZ treatment induced action potential firing in only one of the six CA3 cells examined. Treatment of slices with CTZ, which transiently caused bioluminescence emitted by CA3 cells (Fig. 7*A*), increased the frequency of EPSCs in one out of six recordings from postsynaptic CA1 pyramidal cells (Fig. 7 *B* and *C*). The remaining five cells showed no change in EPSC frequency, consistent with the rate of CTZ-induced action potential firing recorded in presynaptic CA3 pyramidal cells.

Next, we used LMO3 to optically map the circuit between presynaptic CA3 cells and postsynaptic CA1 cells. An example of LMO3 expression in hippocampal dentate gyrus and CA3 neurons and that of a recorded CA1 cell is shown in Fig. 7 *D* and *E*, respectively. Regions within the microscope objective field (~500 μm diameter) were illuminated by scanning a small laser light spot (488 nm) in a random fashion. When the laser spot encountered LMO3-expressing Schaffer collaterals, these axons were photostimulated and light-evoked EPSCs were recorded in the CA1 pyramidal cells (Fig. 7*F*). These light-induced responses reflected glutamatergic EPSCs because they were blocked by treatment with the glutamate receptor antagonists, CNQX (10 μM) plus D-AP5 (50 μM) (Fig. 7*G*), as expected for the CA3–CA1 synapse. All CA1 pyramidal cells examined ($n = 6$) displayed similar light-evoked EPSCs in response to laser activation of Schaffer collaterals. EPSCs were evoked in locations within the stratum radiatum of CA1, where CA3 pyramidal cell axons (Schaffer collaterals) innervate the apical dendrites of CA1 pyramidal cells, but not when the light spot was located in other parts of the hippocampus. Thus, our results provided a functional map of the spatial organization of circuits between CA3 and CA1 neurons.

In summary, these experiments demonstrate that LMO3 enables an integrated opto- and chemogenetic approach, allowing fine-scale mapping of synaptic inputs over a fast time scale (Fig. 7*F*) as well as slower activation of the entire network using a small diffusible molecule (Fig. 7*C*).

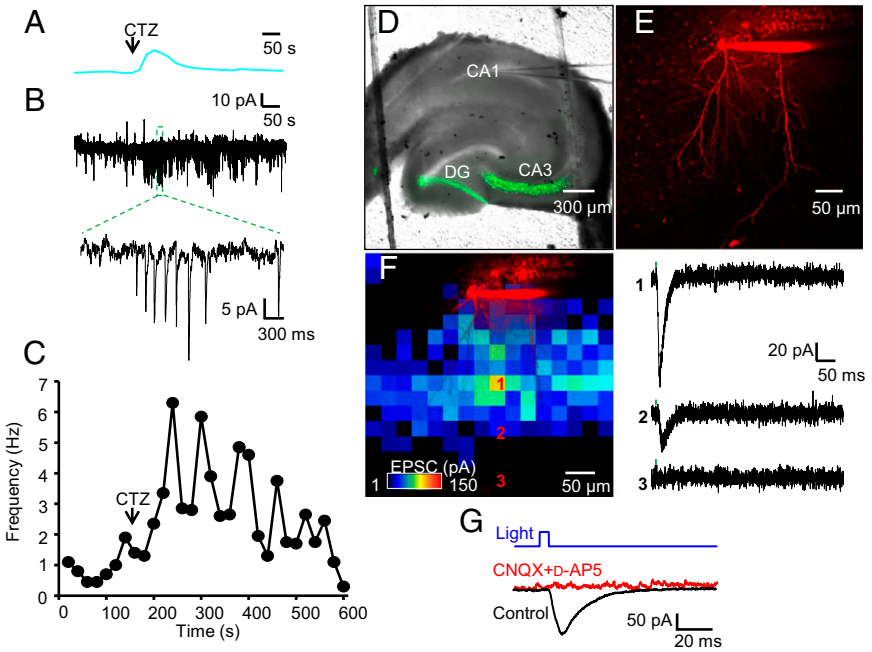

Fig. 7. Bimodal opto- and chemogenetic interrogation of neurons expressing luminopsin. (*A*–*G*) Hippocampal dentate gyrus and CA3 neurons were transduced by AAV-LMO3. (*A*–*C*) CTZ-induced bioluminescence and EPSCs in a CA1 pyramidal cell. CTZ treatment elicited bioluminescence (*A*), as well as fast inward currents, presumably EPSCs. *B*, *Inset* shows inward currents on a faster time scale. (*C*) Time course of CTZ-induced increase in EPSC frequency. (*D*–*G*) Mapping local excitatory inputs of a CA1 pyramidal cell. (*D*) Image shows fluorescence from the EYFP tag (green) overlaid on a bright-field image of a hippocampal slice. (*E*) CA1 pyramidal cell was whole-cell patch clamped with a pipette filled with Texas Red dye, with dye fluorescence revealing morphology of the neuron. (*F*, *Left*) Map of excitatory inputs activated by brief laser light spots scanned throughout the part of the CA1 region shown in *E*. Pseudo color scale (lower left) indicates amplitudes of EPSCs evoked when laser spot was positioned at each location, whereas the red image illustrates cell morphology (from *E*). (*F*, *Right*) Representative EPSCs evoked at locations indicated by corresponding numbers in map at left. (*G*) Light flash (blue) evoked EPSCs (black) that were blocked by treatment with the glutamate receptor antagonists CNQX and D-AP5 (red).

Discussion

We report here the development of luminopsins for in vivo control of behavior in freely moving animals. Although our initial proof-of-concept studies demonstrated that light emitted from wild-type GLuc is able to activate channelrhodopsins when the two molecules are fused together, the resulting CTZ-induced depolarizations were small and subthreshold for action potential firing (3). Here we significantly improved the performance of luminopsins by incorporating brighter versions of GLuc, allowing either suprathreshold depolarization or effective silencing of action potentials when partnered with the appropriate optogenetic elements. We demonstrate this improved luminopsin performance in vitro (Figs. 3 and 4), in vivo (Figs. 5 and 6), and ex vivo (Fig. 7).

We experimentally assessed the effects of several GLuc variants on opsin activation when partnered in a fusion protein and ultimately used two GLuc variants. The one used in LMO3 (sbGLuc) carries two methionine-to-leucine mutations (i.e., M43L and M110L). This mutant was reported to increase the half-life of light emission 10 times over that of wild-type GLuc while preserving the intensity of the luminescence signal (10). The GLuc variant used in iLMO (slGLuc) has one phenylalanine-to-tryptophan and one isoleucine-to-leucine mutation (i.e., F89W and I90L). Compared with wild-type GLuc, this variant has improved quantum yield and faster turnover rates, contributing to 10 times improved bioluminescence intensities (9). Development and refinement of luciferases are ongoing, offering numerous possibilities to improve and tune luminopsins for particular applications (9, 10, 20).

The temporal precision of opsins achieved by physical light activation is an attractive biophysical property. However, many applications, specifically in vivo, often do not require the highest temporal resolution; instead, the usefulness of opsins for in vivo studies within the brain has been limited by the need for optical fibers for light delivery. Reflecting this limitation is the development of optogenetic actuators with red-shifted excitation spectra allowing possible light delivery through the skull (21, 22). However, high-intensity light sources are required to deliver light deep into the brain, which may cause unintended damage near the surface where light energy is high. In contrast, with bioluminescence-driven optogenetics, the cell containing a luminopsin generates its own light just sufficient to activate a nearby opsin. Moreover, any optogenetic element can be paired with a luciferase that matches its spectral properties. Although GLuc variants typically emit blue light, emission spectra of engineered luciferases can be shifted (23–25) and, together with luciferases from different marine organisms (26), can cover a wide spectrum of visible light. This allows the entire optogenetic toolbox to be complemented by a bioluminescence-driven approach.

Luminopsins use a diffusible small molecule for activation, similar to conventional chemogenetic probes such as DREADDs, PSAMs, TRPV1, and others (27–31). The time scales of chemogenetic neuronal modulation, which depend on how fast the small molecule can reach the brain and how fast it dissipates, can be in the range of seconds to hours. In this study, we used two different routes of administration of CTZ—namely, i.v. and i.p. injections. Observed onset times of effect in vivo were within one to several minutes and lasted several minutes to over 30 min, which is shorter than conventional chemogenetic probes such as DREADDs, which typically act from 20 min onset after i.p. injection of the ligand CNO and are sustained over several hours of action. Luminopsins are orthogonal to DREADDs in two other important aspects. First, DREADDs are G protein-coupled receptors and thus require intrinsic intracellular second messenger pathways for their activation. Further, activation of these pathways can potentially cause unintended side effects, such as altering neuronal plasticity. LMOs avoid these complications by using opsins to directly generate electrical current. Second, DREADDs require extended protein engineering, which limits rapid expansion of the toolbox; currently, there is one DREADD for excitation and two for silencing—namely, hM3Dq, hM4Di (32), and hKORD (33). In contrast, LMOs can, in principle, leverage the full array of luciferases, luciferins, and optogenetic elements, offering numerous combinatorial possibilities. In fact, the current study alone demonstrates engineering and evaluation of four new variants of LMOs.

Although several of the individual features of luminopsins overlap with those of current methods, the approach is unique in that luminopsins integrate opto- and chemogenetic approaches, thereby allowing manipulation of neuronal activity over a range of spatial and temporal scales in the same experimental animal. Only luminopsins allow the same opsin to be activated by physical light delivered by a conventional light source or by a systemically injected chemical. Thus, behavioral testing at the macrocircuit level (Figs. 5 and 6) can be complemented by photostimulation mapping at the local microcircuit level in the same experimental animal (Fig. 7 and Figs. S2 and S3). Our approach therefore permits more global and more flexible interrogation of neuronal circuits than is currently possible.

Methods

Constructs. The generation of LMO plasmids is described in detail in ref. 3. For the new versions of LMOs, the wild-type GLuc sequence was replaced by the mutated versions slGLuc (F89W/I90L) (9) or sbGLuc (M43L/M110L) (10) by switching out synthetized sequences (Genscript). *Renilla* luciferase and NanoLuc were retrieved from plasmids provided by Promega. Opsin sequences were cloned from pcDNA3.1/VChR1-EYFP (a gift from Karl Deisseroth, Stanford University, Stanford, CA; Addgene plasmid 20955) and from FCK-Mac-GFP (a gift from Edward Boyden, Massachusetts Institute of Technology, Cambridge, MA; Addgene plasmid 22223). For viral vectors, the coding sequences of LMO3 and iLMO were cloned into a lentiviral or AAV vector downstream of a CAG or hSyn promoter, respectively.

Animals. All experiments were conducted in accordance with approved animal protocols from the Institutional Animal Care and Use Committees of the authors' institutions. Mice had free access to water and food.

Virus. AAVs carrying LMOs were produced by transfecting subconfluent HEK293FT cells per 10-cm culture dish with 24 μg of the helper plasmid pAd delta F6, 20 μg of the serotype plasmid AAV2/9, and 12 μg of the LMO3 plasmid using Lipofectamine 2000. After 72 h, the supernatant was harvested from culture plates and filtered at 0.45 μm. Virus was purified from cells and supernatant following the method of Guo et al. (34), but without the partitioning step in the aqueous two-phase system. Virus was dialyzed against PBS (w/o Ca, Mg) overnight at 4 °C, using FLOAT-A-LYZER G2, MWCO, 50KD, followed by concentration in Amicon Ultra-0.5 mL Centrifugal Filters. Viral titers were determined by quantitative PCR for the woodchuck hepatitis post-transcriptional regulatory element. Preparations with titers ranging from 1×10^7 to 1×10^{10} TU/μL were used in this study.

Lentivirus vectors were made by transfecting 6×10^6 293FT cells with 5 μg of the vesicular stomatitis virus glycoprotein (VSVg) envelope encoding plasmid, 15 μg of the delta-8.9 packaging plasmid, and 20 μg of promoter–reporter plasmid using Lipofectamine 2000. After 72 h, the supernatant was harvested from three 10-cm culture plates, filtered at 0.45 μm, and pelleted by ultracentrifugation at 120,000 × *g* for 2 h at 4 °C. After resuspension, serially diluted lentivirus was used to transduce 293FT cells; 72 h later, labeled 293FT cells were counted to calculate the viral titer. Lentiviruses with titers ranging from 1×10^6 to 1×10^9 TU/ μL were used in this study.

Neuronal Culture. Primary neurons were collected from embryonic day 18 rat embryos carried by pregnant Sprague–Dawley females obtained directly from a commercial vendor (Harlan). Cortical neuron cultures were grown on 12 mm poly-D-lysine–coated coverslips in four-well or 24-well plates. Cells were plated in culture medium consisting of Neurobasal Medium (Invitrogen) containing B-27 (Invitrogen), 2 mM Glutamax (Invitrogen), and 5% FCS. The medium was replaced with culture medium without serum the next day. Neurons were transfected with Lipofectamine 2000 (Invitrogen) or transduced with virus on days in vitro (DIV) 2. Lipofection was done by following the manufacturer's protocol, except that 1/10th of the recommended amount of Lipofectamine was used. Virus was added to the culture medium (1 μL per well of concentrated stocks). All-*trans* retinal (Sigma

R2500) was added to the culture medium to a 100 μM final concentration the day before electrophysiological recordings. Neurons were used for recording on DIV 7–14.

Electrophysiology in Vitro. Cells were examined on an upright epifluorescence microscope (Eclipse FN-1, Nikon) equipped with a 40× 0.8 NA water immersion objective, a metal-halide arc lamp, an electronic shutter (Uniblitz, Vincent Associates), a GFP filter cube (B-2E/C, Nikon), a cooled CCD camera (CoolSNAP fx, Photometrics), and acquisition software (Micro-Manager, https://micro-manager.org/) on a PowerMac G5 (Apple).

For electrophysiology, conventional whole-cell voltage or current clamp recordings were made using a patch clamp amplifier (Multiclamp 700B; Axon Instruments), a digital acquisition system (Digidata 1440A; Axon Instruments), and pClamp 10 software (Axon Instruments) on a PC. Recording pipettes had resistances of 7–10 MΩ when filled with 140 mM K-gluconate, 2 mM $MgCl_2$, 0.5 mM $CaCl_2$, 10 mM Hepes, 4 mM Na_2-ATP, 0.4 mM Na_3-GTP, and 5 mM EGTA (pH 7.1 titrated with KOH). In some experiments, $[Cl^-]$ was increased to 12.5 mM by substituting 7.5 mM of K-gluconate with equimolar KCl. The extracellular solution consisted of 150 mM NaCl, 3 mM KCl, 2 mM $CaCl_2$, 2 mM $MgCl_2$, 20 mM D-glucose, and 10 mM Hepes (pH 7.35, titrated with NaOH). For voltage clamp experiments, cells were held at –60 mV. For current clamp experiments, cells were held with zero current. Junction potential was not corrected. A chamber for a 12-mm coverslip (RC-48LP, Warner Instruments) was constantly superfused with the extracellular solution at ∼500 μL/min. For routine opsin photoactivation, the GFP filter cube (excitation, 465–495 nm) was used. All of the experiments were performed at room temperature (21–24 °C).

Bioluminescence Imaging. The GLuc substrate CTZ was purchased from Nanolight Technology. CTZ free base, the natural form of CTZ (Nanolight, cat. no. 303), was reconstituted in Nanolight's proprietary solvent NanoFuel (cat. no. 399; 0.5 mg/50 μL) and kept at –80 °C. The NanoLuc substrate, furimazine, was purchased from Promega.

For measuring luminescence from HEK cells, reconstituted and diluted CTZ was added to the culture medium to the final concentration indicated in the experiment. Bioluminescence was measured from each well of a 96-well plate using a plate reader (GloMax, Promega).

For recording experiments, reconstituted CTZ was diluted in the extracellular solution at 100 μM immediately before the experiments. CTZ solution (∼0.5 mL) was added to the recording chamber immediately before imaging. Bioluminescence was imaged using the CCD camera every 5 s without any filter cube with 4-by-4 binning and 4.5-s exposure.

Stereotactic Injection of Virus. Mice (C57BL/6) used for collection of brain slices were injected with AAV-LMO3 into the hippocampus. Animals were anesthetized by i.p. injections of ketamine/xylazine mixture and placed in a stereotaxic apparatus (David Kopf Instruments). For injection of viruses, a 31-gauge syringe needle was used to infuse 2 μL of virus into the dentate gyrus and CA3 of the hippocampus at a rate of 0.1 μL/min. The needle was left in place for 10 min after injection before being slowly withdrawn. To close the incision, Vetbond tissue adhesive (3 M, 7003449) was used. After surgery, mice were given analgesia.

For virus injection in the SNr, mice implanted with indwelling stainless steel guide cannulas (24 g; Plastics One) unilaterally aimed at the SNr were injected with 0.6 μL AAV-hSyn-LMO3 or AAV-hSyn-iLMO using a Hamilton syringe over 6 min and left in place for 5 min postinjection to allow for diffusion away from the injection site.

Slice Preparations and Electrophysiology. Hippocampal slices were prepared, using conventional methods (35), 2–3 wk after virus injection. In brief, the mice were anesthetized, their brains were isolated and then placed in cold artificial cerebrospinal fluid, containing (in mM) 125 NaCl, 2.5 KCl, 1.25 NaH_2PO_4, 26 $NaHCO_3$, 20 d(+)-glucose, 2 $CaCl_2$ and 1.3 $MgCl_2$ (pH 7.4 after bubbling with 95% O_2/ 5% CO_2, vol/vol). A vibratome was used to make 300-μm-thick coronal sections. The slices were then incubated at 36 °C for 30 min before use.

Electrophysiological recording in slices was done with IR-DIC and 2-photon imaging, using an Olympus FV1000 microscope, similar to our previous study (36). In brief, fluorescence was excited with 790 nm light (<50 mW) and imaged using either a 25× or 40× water-immersion objective (Olympus) with appropriate emission filters for EYFP and Alexa Fluor 594 (Invitrogen). Whole-cell patch clamp recording was made similar to in vitro recording with a glass pipette of lower resistance (2–7 MΩ) and Alexa Fluor 594. For photostimulation, an area of ∼500 × 500 μm was scanned with a 488-nm laser spot (typically 4 ms duration) in a 32 × 32 array of pixels. The laser spot was scanned in a pseudorandom sequence, to avoid activation of adjacent pixels, while cellular responses were simultaneously measured with whole-cell patch clamp recordings (37).

In Vivo Electrophysiology. Each mouse was fully anesthetized with isoflurane (induction at 3%, maintained at 1%). The head was fixed on a stereotax (Kopf) for a craniotomy (∼1 mm × 2 mm) to target the SNr. The dura was first removed, and the virus was injected (five mice each for LMO3 and for iLMO). The electrode arrays were inserted into place, targeting the final coordinates (in mm relative to Bregma): anterior-posterior, –3.4; medial-lateral, ±1.25; dorsal-ventral, –4.9. Each array contained 16 tungsten microwires (5–7 mm, 50 μm) with 150-μm electrode spacing and 200-μm row spacing attached to an Omnetics connector in a 4 × 4 configuration (Innovative Electrophysiology). The arrays were grounded to screws placed in the skull with a silver ground wire and then anchored in place with dental acrylic. After surgery, mice were allowed to recover for at least 1 wk before starting the recording experiments. Single unit activity was recorded using the Cerebus data acquisition system (Blackrock).

Data were filtered with analog and digital band-pass filters (analog high-pass first order Butterworth filter at 0.3 Hz, analog low-pass third order Butterworth filter at 7.5 kHz). Data were filtered with analog and digital band-pass filters (analog high-pass first order Butterworth filter at 0.3 Hz, analog low-pass third order Butterworth filter at 7.5 kHz) and then separated with a high-pass digital filter (fourth order Butterworth filter at 250 Hz) and sampled at 30 kHz. The data were processed using online sorting algorithms and then resorted offline (Offline Sorter, Plexon). Waveforms were classified as single units as previously described (38–40). The following criteria were used: (*i*) a signal to noise ratio of at least 3:1, (*ii*) consistent waveforms throughout the recording session, and (*iii*) refractory period of at least 1,000 μs. Data were analyzed using Neuroexplorer.

Behavioral Experiments. For application of CTZ directly through the cannula, injectors were lowered extending 0.2 mm past the end of the cannulas, which were implanted using the same stereotaxic coordinates as for the electrode arrays. PBS (control) or CTZ in saline (34 ng; 400 nL) was injected at a rate of 0.15 μL/min by a Harvard Apparatus injector pump. For systemic CTZ application, mice were injected into the tail vein with 200 μg CTZ in 50 μL solvent. Mice were placed in the experimental chamber, and behavior was monitored via video recording. Mice were recorded for 10 min. The number of ipsiversive and contraversive turns was counted. Anatomical location was verified at the end of the experiments by fluorescence microscopy of perfused and sectioned brains.

Statistical Analyses. All analyses and statistics were done in Igor Pro-6 (WaveMetrics), using in-house and NeuroMatic macros (Jason Rothman) for electrophysiological data and/or Origin 8 software.

ACKNOWLEDGMENTS. This work was supported by National Institutes of Health Grant R21MH101525 (to U.H.), a Duke Institute for Brain Science Research Incubator Award (to U.H., H.H.Y., and Dr. Marc A. Sommer), and a German Academic Exchange Program–Research Internships in Science and Engineering Research Fellowship (to J.G.).

1. Fenno L, Yizhar O, Deisseroth K (2011) The development and application of optogenetics. *Annu Rev Neurosci* 34:389–412.
2. Sternson SM, Roth BL (2014) Chemogenetic tools to interrogate brain functions. *Annu Rev Neurosci* 37:387–407.
3. Berglund K, Birkner E, Augustine GJ, Hochgeschwender U (2013) Light-emitting channelrhodopsins for combined optogenetic and chemical-genetic control of neurons. *PLoS One* 8(3):e59759.
4. Birkner E, Berglund K, Klein ME, Augustine GJ, Hochgeschwender U (March 5, 2014) Non-invasive activation of optogenetic actuators. *SPIE Proc* 8928:89282F.
5. Ernst OP, et al. (2008) Photoactivation of channelrhodopsin. *J Biol Chem* 283(3):1637–1643.
6. Zhang F, et al. (2008) Red-shifted optogenetic excitation: A tool for fast neural control derived from Volvox carteri. *Nat Neurosci* 11(6):631–633.
7. Verhaegent M, Christopoulos TK (2002) Recombinant Gaussia luciferase. Overexpression, purification, and analytical application of a bioluminescent reporter for DNA hybridization. *Anal Chem* 74(17):4378–4385.
8. Tannous BA, Kim D-E, Fernandez JL, Weissleder R, Breakefield XO (2005) Codon-optimized Gaussia luciferase cDNA for mammalian gene expression in culture and in vivo. *Mol Ther* 11(3):435–443.
9. Kim SB, Suzuki H, Sato M, Tao H (2011) Superluminescent variants of marine luciferases for bioassays. *Anal Chem* 83(22):8732–8740.
10. Welsh JP, Patel KG, Manthiram K, Swartz JR (2009) Multiply mutated Gaussia luciferases provide prolonged and intense bioluminescence. *Biochem Biophys Res Commun* 389(4):563–568.
11. Hall MP, et al. (2012) Engineered luciferase reporter from a deep sea shrimp utilizing a novel imidazopyrazinone substrate. *ACS Chem Biol* 7(11):1848–1857.

12. Stacer AC, et al. (2013) NanoLuc reporter for dual luciferase imaging in living animals. *Mol Imaging* 12(7):1–13.
13. Chow BY, et al. (2010) High-performance genetically targetable optical neural silencing by light-driven proton pumps. *Nature* 463(7277):98–102.
14. Tung JK, Gutekunst CA, Gross RE (2015) Inhibitory luminopsins: Genetically-encoded bioluminescent opsins for versatile, scalable, and hardware-independent optogenetic inhibition. *Sci Rep* 5:14366.
15. Kilpatrick IC, Collingridge GL, Starr MS (1982) Evidence for the participation of nigrotectal gamma-aminobutyrate-containing neurones in striatal and nigral-derived circling in the rat. *Neuroscience* 7(1):207–222.
16. Grace AA, Onn SP (1989) Morphology and electrophysiological properties of immunocytochemically identified rat dopamine neurons recorded in vitro. *J Neurosci* 9(10): 3463–3481.
17. Grace AA, Bunney BS (1979) Paradoxical GABA excitation of nigral dopaminergic cells: Indirect mediation through reticulata inhibitory neurons. *Eur J Pharmacol* 59(3-4): 211–218.
18. Hajós M, Greenfield SA (1993) Topographic heterogeneity of substantia nigra neurons: Diversity in intrinsic membrane properties and synaptic inputs. *Neuroscience* 55(4):919–934.
19. Tepper JM, Martin LP, Anderson DR (1995) GABAA receptor-mediated inhibition of rat substantia nigra dopaminergic neurons by pars reticulata projection neurons. *J Neurosci* 15(4):3092–3103.
20. Degeling MH, et al. (2013) Directed molecular evolution reveals Gaussia luciferase variants with enhanced light output stability. *Anal Chem* 85(5):3006–3012.
21. Lin JY, Knutsen PM, Muller A, Kleinfeld D, Tsien RY (2013) ReaChR: A red-shifted variant of channelrhodopsin enables deep transcranial optogenetic excitation. *Nat Neurosci* 16(10):1499–1508.
22. Chuong AS, et al. (2014) Noninvasive optical inhibition with a red-shifted microbial rhodopsin. *Nat Neurosci* 17(8):1123–1129.
23. Loening AM, Wu AM, Gambhir SS (2007) Red-shifted Renilla reniformis luciferase variants for imaging in living subjects. *Nat Methods* 4(8):641–643.
24. Saito K, et al. (2012) Luminescent proteins for high-speed single-cell and whole-body imaging. *Nat Commun* 3:1262.
25. Takai A, et al. (2015) Expanded palette of Nano-lanterns for real-time multicolor luminescence imaging. *Proc Natl Acad Sci USA* 112(14):4352–4356.
26. Haddock SHD, Moline MA, Case JF (2010) Bioluminescence in the sea. *Annu Rev Mar Sci* 2:443–493.
27. Lechner HAE, Lein ES, Callaway EM (2002) A genetic method for selective and quickly reversible silencing of Mammalian neurons. *J Neurosci* 22(13):5287–5290.
28. Lerchner W, et al. (2007) Reversible silencing of neuronal excitability in behaving mice by a genetically targeted, ivermectin-gated Cl- channel. *Neuron* 54(1):35–49.
29. Armbruster BN, Li X, Pausch MH, Herlitze S, Roth BL (2007) Evolving the lock to fit the key to create a family of G protein-coupled receptors potently activated by an inert ligand. *Proc Natl Acad Sci USA* 104(12):5163–5168.
30. Magnus CJ, et al. (2011) Chemical and genetic engineering of selective ion channel-ligand interactions. *Science* 333(6047):1292–1296.
31. Güler AD, et al. (2012) Transient activation of specific neurons in mice by selective expression of the capsaicin receptor. *Nat Commun* 3:746.
32. Zhu H, Roth BL (2015) DREADD: A chemogenetic GPCR signaling platform. *Int J Neuropsychopharmacol* 18(1):1–6.
33. Vardy E, et al. (2015) A new DREADD facilitates the multiplexed chemogenetic interrogation of behavior. *Neuron* 86(4):936–946.
34. Guo P, et al. (2012) Rapid and simplified purification of recombinant adeno-associated virus. *J Virol Methods* 183(2):139–146.
35. Tanaka K, et al. (2007) Ca^{2+} requirements for cerebellar long-term synaptic depression: Role for a postsynaptic leaky integrator. *Neuron* 54(5):787–800.
36. Asrican B, et al. (2013) Next-generation transgenic mice for optogenetic analysis of neural circuits. *Front Neural Circuits* 7:160.
37. Wang H, et al. (2007) High-speed mapping of synaptic connectivity using photostimulation in Channelrhodopsin-2 transgenic mice. *Proc Natl Acad Sci USA* 104(19): 8143–8148.
38. Fan D, Rossi MA, Yin HH (2012) Mechanisms of action selection and timing in substantia nigra neurons. *J Neurosci* 32(16):5534–5548.
39. Rossi MA, Fan D, Barter JW, Yin HH (2013) Bidirectional modulation of substantia nigra activity by motivational state. *PLoS One* 8(8):e71598.
40. Barter JW, Castro S, Sukharnikova T, Rossi MA, Yin HH (2014) The role of the substantia nigra in posture control. *Eur J Neurosci* 39(9):1465–1473.